

THE FIRST STELLAR CLUSTER

PAUL C. CLARK¹, SIMON C. O. GLOVER², RALF S. KLESSEN¹

¹Zentrum für Astronomie der Universität Heidelberg, Institut für Theoretische Astrophysik, Albert-Ueberle-Str. 2, 69120 Heidelberg, Germany

email: pcc@ita.uni-heidelberg.de, rklessen@ita.uni-heidelberg.de

²Astrophysikalisches Institut Potsdam, An der Sternwarte 16, D-14482 Potsdam, Germany
email: sglover@aip.de

Draft version November 4, 2018

ABSTRACT

We report results from numerical simulations of star formation in the early universe that focus on gas at very high densities and very low metallicities. We argue that the gas in the central regions of protogalactic halos will fragment as long as it carries sufficient angular momentum. Rotation leads to the build-up of massive disk-like structures which fragment to form protostars. At metallicities $Z \approx 10^{-5} Z_{\odot}$, dust cooling becomes effective and leads to a sudden drop of temperature at densities above $n = 10^{12} \text{ cm}^{-3}$. This induces vigorous fragmentation, leading to a very densely-packed cluster of low-mass stars. This is the first stellar cluster. The mass function of stars peaks below $1 M_{\odot}$, similar to what is found in the solar neighborhood, and comparable to the masses of the very-low metallicity subgiant stars recently discovered in the halo of our Milky Way. We find that even purely primordial gas can fragment at densities $10^{14} \text{ cm}^{-3} \leq n \leq 10^{16} \text{ cm}^{-3}$, although the resulting mass function contains only a few objects (at least a factor of ten less than the $Z = 10^{-5} Z_{\odot}$ mass function), and is biased towards higher masses. A similar result is found for gas with $Z = 10^{-6} Z_{\odot}$. Gas with $Z \leq 10^{-6} Z_{\odot}$ behaves roughly isothermally at these densities (with polytropic exponent $\gamma \approx 1.06$) and the massive disk-like structures that form due to angular momentum conservation will be marginally unstable. As fragmentation is less efficient, we expect stars with $Z \leq 10^{-6} Z_{\odot}$ to be massive, with masses in excess of several tens of solar masses, consistent with the results from previous studies.

Subject headings: stars: formation – stars: mass function – early universe – hydrodynamics – equation of state – methods: numerical

1. INTRODUCTION

Detailed numerical simulations of the formation of the first stars, the so-called population III stars, indicate that they were probably massive, with masses greater than $20 M_{\odot}$ (Abel, Bryan, & Norman 2002; Bromm, Coppi, & Larson 2002; Yoshida *et al.* 2006; O’Shea & Norman 2007). The fact that no population III star has ever been observed in the Milky Way provides some observational support for this prediction (Tumlinson 2006). However, a number of low-mass, extremely metal-poor, stars with $[\text{Fe}/\text{H}] < -3$ have been discovered in the Galactic halo (Beers & Christlieb 2005), suggesting that the distribution of stellar masses is sensitive to even very low levels of metal enrichment. Explanations of this apparent change in the IMF have concentrated on the fact that metal-enriched gas has more coolants than its primordial counterpart. These coolants are suggested to provide an opportunity for efficient fragmentation, since they can keep the gas temperature lower during the collapse process than is possible with pure H_2 cooling in the primordial gas. If this is the case, then the final IMF will likely contain at least some low-mass stars, even if it still differs significantly from the present-day local IMF.

If metal enrichment is the key to the formation of low-mass stars, then logically there must be some critical metallicity Z_{crit} at which the formation of low mass stars first becomes possible. However, the value of Z_{crit} is a matter of ongoing debate. Some models suggest that low mass star formation becomes possible only once atomic fine-structure line cooling from

carbon and oxygen becomes effective (Bromm *et al.* 2001; Bromm & Loeb 2003; Santoro & Shull 2006; Frebel, Johnson, & Bromm 2007), setting a value for Z_{crit} at around $10^{-3.5} Z_{\odot}$. Another possibility, and the one that we explore with this paper, is that low mass star formation is a result of dust-induced fragmentation occurring at high densities, and thus at a very late stage in the protostellar collapse (Schneider *et al.* 2002; Omukai *et al.* 2005; Schneider *et al.* 2006). In this model, $10^{-6} \lesssim Z_{\text{crit}} \lesssim 10^{-4} Z_{\odot}$, where much of the uncertainty in the predicted value results from uncertainties in the dust composition and the degree of gas-phase depletion (Schneider *et al.* 2002, 2006).

The recent simulations performed by Tsuribe & Omukai (2006), which model the collapse of very high density protogalactic gas, provide some support for the dust-induced fragmentation model. Using a simple piecewise polytropic equation of state to describe the thermal evolution of extremely metal-poor protogalactic gas, Tsuribe & Omukai (2006) show that fragmentation can occur at metallicities as low as $Z = 10^{-6} Z_{\odot}$, and that it becomes more effective as the metallicity increases. However, their study considered only the limiting case of gas with zero angular momentum. Owing to the absence of angular momentum, the fragments formed in their simulation do not survive for longer than a dynamical time, as they simply fall to the center of the potential well, where they merge with other fragments. It is also unclear whether the fragmentation process would be as effective if the angular momentum of the gas were non-zero, as would be expected in reality.

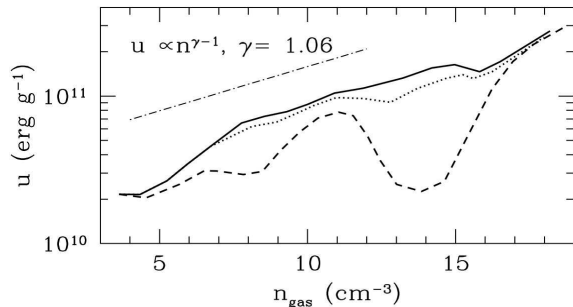


FIG. 1.— The three equations of state (EOSs) from Omukai et al. (2005) that are used in our study. The primordial case (solid line), $Z = 10^{-6} Z_{\odot}$ (dotted line), and $Z = 10^{-5} Z_{\odot}$ (dashed line), are shown alongside an example of a polytropic EOS with an effective $\gamma = 1.06$.

We present the results of simulations of the high-density, dust-cooling dominated regime that improve on those of Tsuribe & Omukai (2006) by including the effects of rotation, and by following a much larger dynamical range of the collapse (ten orders of magnitude in density), as well as employing an equation of state (EOS) which follows that of Omukai et al. (2005) more closely. We also perform some simulations of purely primordial gas for comparison. A key feature is the use of sink particles (Bate, Bonnell & Price 1995) to capture the formation and evolution of multiple collapsing cores, which enables us to follow the evolution of the star-forming gas over several free-fall timescales and thus to model the build-up of a stellar cluster. This differs from previous calculations which either follow the collapse of a single core to high densities (Abel, Bryan, & Norman 2002; Bromm & Loeb 2004; Yoshida *et al.* 2006), or use sink particles to capture low density ($n < 10^6 \text{ cm}^{-3}$) fragmentation (e.g. Bromm, Coppi, & Larson 2002).

In following section, we give details of the numerical model (§2.1) and the initial set-up of the simulations (§2.2). The main results of our study are presented in §3 and we discuss the origin of the fragmentation in §4. Potential caveats with the current model are highlighted in §5, and there is a summary of our findings in §6.

2. DETAILS OF THE CALCULATIONS

2.1. Numerical Method

We follow the evolution of the gas in this study using Smoothed Particle Hydrodynamics (SPH). Our version of the code is essentially a parallelized version of that used by Bate et al. (1995), which utilizes adaptive smoothing lengths for the gas particles and a binary tree algorithm for computing gravitational forces and constructing SPH neighbor lists. The calculations were performed on the Jülich Multi-processor (JUMP) supercomputer at the John von Neumann Institute for Computing, Research Center Jülich, Germany.

The thermal evolution of the gas in our simulations is modelled using a tabulated equation of state (EOS) that is based on the results of the detailed chemical modelling of Omukai et al. (2005). We use their reported results for the temperature and molecular fraction as functions of gas density (their Figures 1 & 3) with metallicities $Z = 0$, 10^{-6} and $10^{-5} Z_{\odot}$ to compute the internal energy density

and thermal pressure of the gas at a range of different densities. These values are used to construct look-up tables which are then used by the SPH code to compute the pressure and internal energy at any required density, for a given gas metallicity, via linear interpolation (in log-log space) between the tabulated values. The resulting equations of state are plotted in Figure 1. By using a tabulated equation of state, we avoid the large computational expense involved in solving the full thermal energy equation, while still obtaining qualitatively correct behavior.

To model the star formation in this study we use sink particles, as described by Bate et al. (1995). This involves replacing the innermost parts of dense, self-gravitating regions of gas with particles that can both accrete further material from their surroundings and interact with other particles in the simulation via gravity. Sink particles are formed once an SPH particle and its neighbors are gravitationally bound, collapsing (negative velocity divergence), and within an accretion radius, h_{acc} , which is taken here to be 0.4 AU. Gravitational interactions between the sink particles and all other particles in the simulation are also smoothed, self-consistently, to h_{acc} . Our set-up allows us to identify sink particles as the direct progenitors of individual stars (for a more detailed discussion, see e.g. Wuchterl & Klessen 2001).

2.2. Setup and Initial conditions

Our calculations are designed to start from the point where previous fragmentation calculations ended. It is now well established that the gas which falls into collapsing dark matter mini-halos undergoes a phase of fragmentation, resulting in the formation of large, self-gravitating clumps, with masses of order $100 M_{\odot}$. The origin of this fragmentation is the rapid cooling driven by H_2 that occurs at densities of around $10 - 10^4 \text{ cm}^{-3}$, and the masses of the clumps are similar to the Jeans mass at the corresponding density and temperature in this regime. We thus pick up the evolution from conditions similar to those reached in the study of Bromm et al. (2001). Since the process of chemical enrichment involves supernovae events from the first stars we expect the gas to have a certain initial level of turbulence, which is normally assumed to be absent during the formation of the very first stars from purely primordial gas. We also adopt a net angular momentum for the gas consistent with the results of simulations of cosmological structure formation.

The clouds in this study have a mass of $500 M_{\odot}$, and are modelled using either 2 million or 25 million SPH particles. In the higher resolution calculations, this gives a particle mass of $2 \times 10^{-5} M_{\odot}$ and a mass resolution of $0.002 M_{\odot}$ (Bate & Burkert 1997), roughly 10 times smaller than the opacity limit set by the Omukai et al. (2005) equation of state. These simulations therefore have roughly an order of magnitude of surplus resolution. The low-resolution calculations have a mass resolution roughly equal to the mass at which the gas becomes optically thick. To ensure that the Jeans condition is not violated, the sinks are always formed just before the optically thick regime in all the simulations. Our clouds have an initial radius of 0.17pc, at an initial uniform density of $5 \times 10^5 \text{ cm}^{-3}$. This corresponds to an initial free-fall time of $t_{ff} = (3\pi/32G\pi\rho)^{1/2} = 5.1 \times 10^4$ years. At this scale

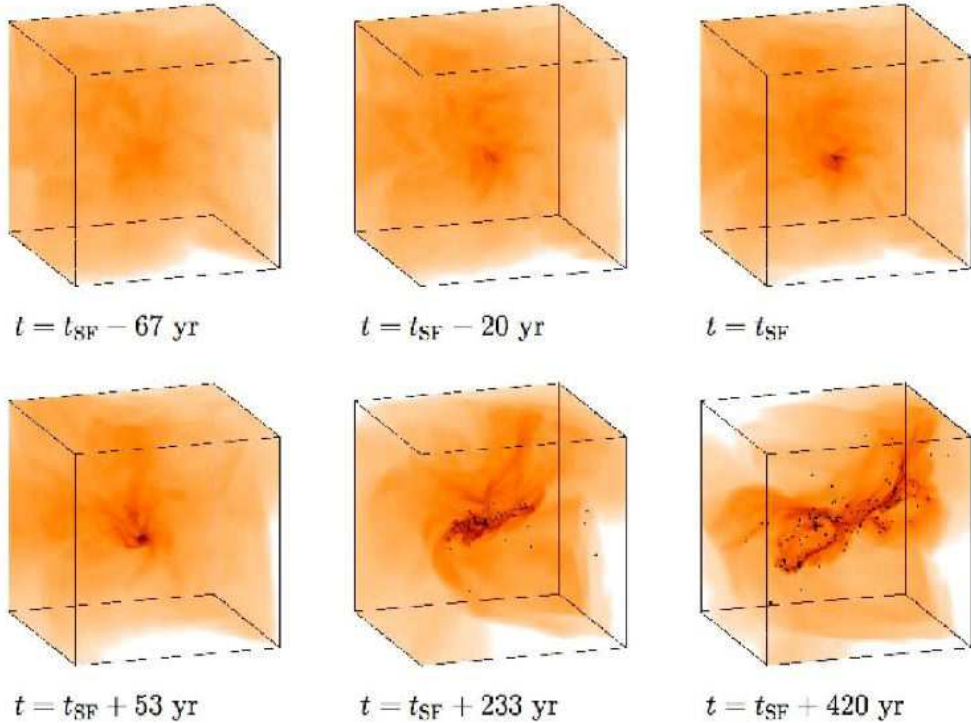


FIG. 2.— Time evolution of the density distribution in the innermost 400 AU of the protogalactic halo shortly before and shortly after the formation of the first protostar at t_{SF} . We plot only gas at densities above 10^{10} cm^{-3} . The dynamical timescale at a density $n = 10^{13} \text{ cm}^{-3}$ is of the order of only 10 years. Dark dots indicate the location of protostars as identified by sink particles forming at $n \geq 10^{17} \text{ cm}^{-3}$. Note that without usage of sink particles we would not have been able to follow the build-up of the protostellar cluster beyond the formation of the first object. There are 177 protostars when we stop the calculation at $t = t_{\text{SF}} + 420 \text{ yr}$. They occupy a region roughly a hundredth of the size of the initial cloud. With $18.7 M_{\odot}$ accreted at this stage, the stellar density is $2.25 \times 10^9 M_{\odot} \text{ pc}^{-3}$.

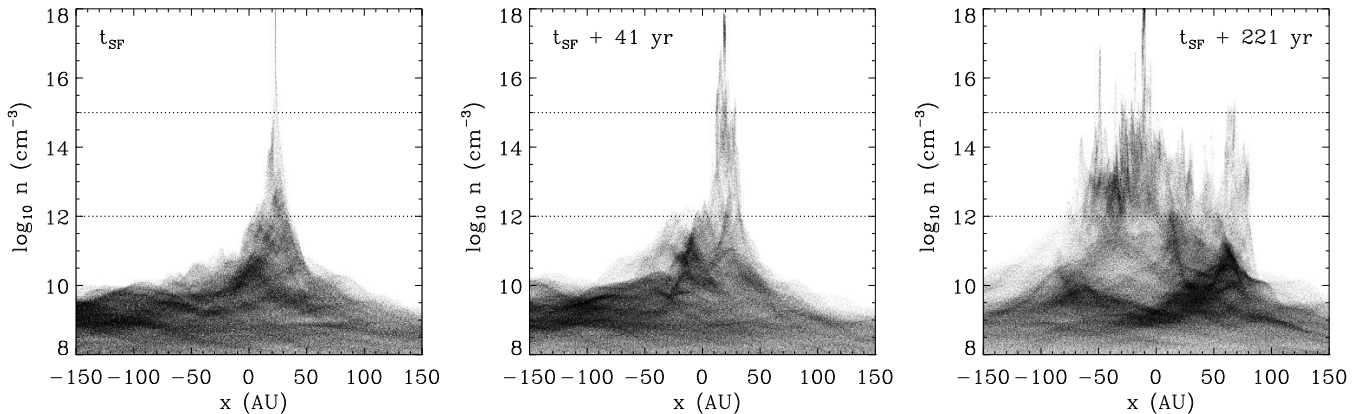


FIG. 3.— We illustrate the onset of the fragmentation process in the high resolution $Z = 10^{-5} Z_{\odot}$ simulation. The graphs show the densities of the particles, plotted as a function of their x -position. Note that for each plot, the particle data has been centered on the region of interest. We show here results at three different output times, ranging from the time that the first star forms (t_{SF}) to 221 years afterwards. The densities lying between the two horizontal dashed lines denote the range over which dust cooling lowers the gas temperature.

and density regime, the contributions from dark matter to the gravitational potential are small and are thus not taken into account in our computational set up. One can see from Figure 1 that the different gas metallicities have slightly different internal energies at the starting density. Thus, the $Z \leq 10^{-6} Z_{\odot}$ calculations have an initial ratio of thermal to gravitational energy of $\alpha = E_{\text{therm}}/|E_{\text{grav}}| = 0.39$, while the cooler $Z = 10^{-5} Z_{\odot}$ cal-

culations have an initial value of $\alpha = 0.32$. All simulations are given a low level of initial turbulence, with the ratio of turbulent to gravitational potential energy $E_{\text{turb}}/|E_{\text{grav}}| = 0.1$, and thus an RMS Mach number of $\mathcal{M}_{\text{RMS}} \approx 1$. The clouds are set in initially uniform rotation, with $\beta = E_{\text{rot}}/|E_{\text{grav}}| = 0.02$. The conditions at the start of our simulation are thus similar to those at which Bromm, Coppi, & Larson (2002) form their sink

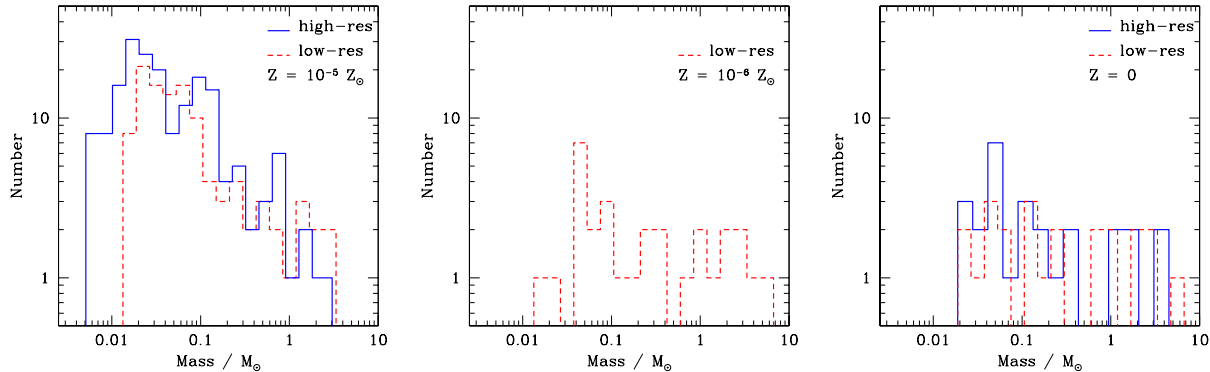


FIG. 4.— Mass functions resulting from simulations with metallicities $Z = 10^{-5} Z_{\odot}$ (left-hand panel), $Z = 10^{-6} Z_{\odot}$ (center panel), and $Z = 0$ (right-hand panel). The plots refer to the point in each simulation at which $19 M_{\odot}$ of material has been accreted (which occurs at a slightly different time in each simulation). The mass resolutions are $0.002 M_{\odot}$ and $0.025 M_{\odot}$ for the high and low resolution simulations, respectively. Note the similarity between the results of the low-resolution and high-resolution simulations. The onset of dust-cooling in the $Z = 10^{-5} Z_{\odot}$ cloud results in a stellar cluster which has a mass function similar to that for present day stars, in that the majority of the mass resides in the lower-mass objects. This contrasts with the $Z = 10^{-6} Z_{\odot}$ and primordial clouds, in which the bulk of the cluster mass is in high-mass stars.

particles (see their Figure 5 for comparison). We perform low-resolution simulations for all three metallicity cases, and high-resolution simulations for the primordial and $Z = 10^{-5} Z_{\odot}$ cases.

3. RESULTS

We find that enrichment of the gas to a metallicity of only $Z = 10^{-5} Z_{\odot}$ dramatically enhances fragmentation within the dense, collapsing cloud. We first focus our discussion on the evolution of the $Z = 10^{-5} Z_{\odot}$ gas cloud, before contrasting with the $10^{-6} Z_{\odot}$ and primordial clouds.

The evolution of the high-resolution $Z = 10^{-5} Z_{\odot}$ simulation is illustrated in Figure 2, in a series of snapshots showing the density distribution of the gas. We show several stages in the collapse process, spanning a time interval from shortly before the formation of the first protostar (as identified by the formation of a sink particle in the simulation) to 420 years afterwards. Note that we show only the innermost 1% of the full computational domain. A complementary view is given in Figure 3, which shows the particle densities as a function of position.

During the initial contraction, the cloud builds up a central core with a density of about $n = 10^{10} \text{ cm}^{-3}$. This core is supported by a combination of thermal pressure and rotation. Eventually, the core reaches high enough densities to go into free-fall collapse, and forms a single protostar. As more high angular momentum material falls to the center, the core evolves into a disk-like structure with density inhomogeneities caused by low levels of turbulence. As it grows in mass, its density increases. When dust-induced cooling sets in, it fragments heavily into a tightly packed protostellar cluster within only a few hundred years. One can see this behavior in particle density-position plots in Figure 3. We stop the simulation 420 years after the formation of the first stellar object (sink particle). At this point, the core has formed 177 stars. The evolution in the low-resolution simulation is very similar. The time between the formation of the first and second protostars is roughly 23 years, which is two orders of magnitude higher than the free-fall time at

the density where the sinks are formed. Without the inclusion of sink particles, we would only have been able to capture the formation of the first collapsing object which forms the first protostar: *the formation of the accompanying cluster would have been missed entirely.*

The mass functions of the protostars at the end of the $Z = 10^{-5} Z_{\odot}$ simulations (both high and low resolution cases) are shown in Figure 4 (left-hand panel). When our simulation is terminated, the sink particles hold $\sim 19 M_{\odot}$ of gas in total. The mass function peaks somewhere below $0.1 M_{\odot}$ and ranges from below $0.01 M_{\odot}$ to about $5 M_{\odot}$. It is important to stress here that this is not the final protostellar mass function. The continuing accretion of gas by the cluster will alter the mass function, as will mergers between the newly-formed protostars (which cannot be followed using our current sink particle implementation). Protostellar feedback in the form of winds, jets and HII regions may also play a role in determining the shape of the final stellar mass function. However, a key point to note is that the chaotic evolution of a bound system such as this cluster ensures that a wide spread of stellar masses will persist. Some stars will enjoy favourable accretion at the expense of others that will be thrown out of the system (as can be seen in Figure 2), thus having their accretion effectively terminated (see for example, the discussions in Bonnell & Bate 2006 and Bonnell, Larson & Zinnecker 2007). The survival of some of the low mass stars formed in the cluster is therefore inevitable.

Our calculations demonstrate that the dust-cooling model of Omukai et al. (2005) can indeed lead to the formation of low-mass objects from gas with very low metallicity. This suggests that the transition from high-mass primordial stars to Population II stars with a more “normal” mass spectrum occurs early in the universe, at metallicities at or below $Z \approx 10^{-5} Z_{\odot}$. Our simulations even predict the existence of brown dwarfs in this metallicity range. Their discovery would be a critical test for our model of the formation of the first star cluster. The first hints of its validity come from the very low metallicity sub-giant stars that have recently been

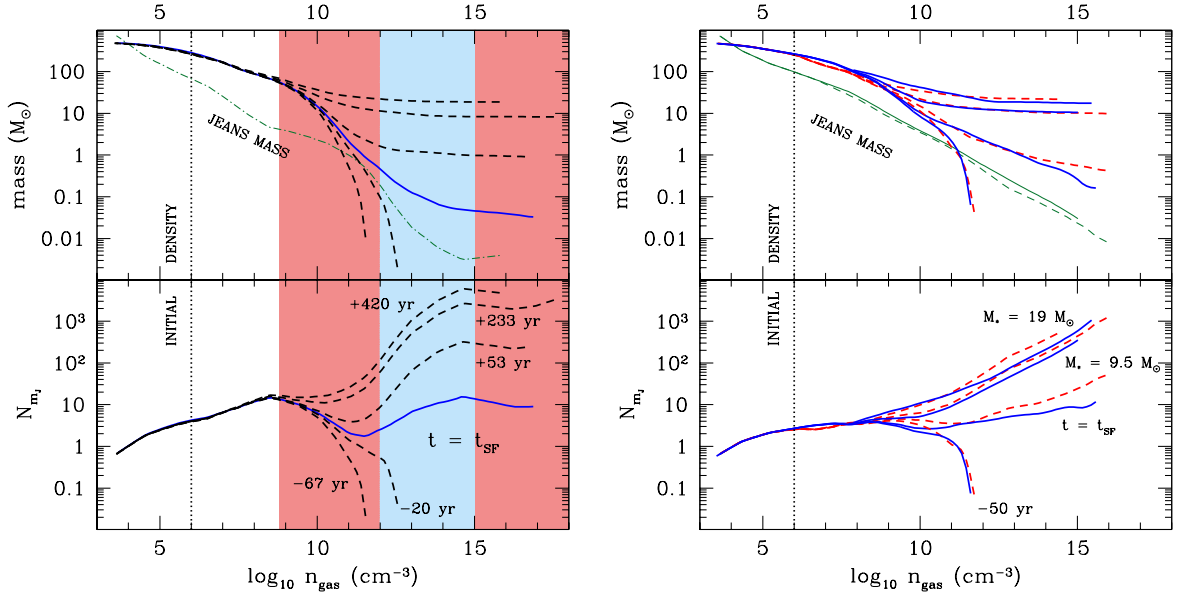


FIG. 5.— The mass (upper panels) and the number of Jeans masses (lower panels) are both shown here as a function of gas density, with the high-resolution $Z = 10^{-5} Z_{\odot}$ simulation in the left-hand plot and both the high-resolution primordial and low-resolution $Z = 10^{-6} Z_{\odot}$ simulations in the right-hand plot. In the upper panels, we plot the mass residing above a density, n_{gas} , as a function of that density, as well as the Jeans mass. In the lower panels, we plot the number of Jeans masses as a function of density. In the left-hand panel, we show via the shaded areas, the heating (pink) and cooling (light blue) phases in the $Z = 10^{-5} Z_{\odot}$ EOS. In the right-hand plot, we show the conditions in the primordial (high-resolution) simulation (solid lines), and $Z = 10^{-6} Z_{\odot}$ simulation (dashed lines). The gas conditions are shown at the point of star formation and 50 years earlier, as well as at two instants after star formation, when the clouds have converted around $9.5 M_{\odot}$ and $19 M_{\odot}$ of gas into protostars. Note that we only label the evolutionary stages in the lower panels, but the same progression with time, going from lower left-most lines to those at the top, applies also to the upper panels.

discovered in the Galactic halo (Christlieb et al. 2002; Beers & Christlieb 2005), which have iron abundances less than 10^{-5} times the solar value and masses below one solar mass, consistent with the range reported here.

Turning our attention to the $Z = 0$ and $Z = 10^{-6} Z_{\odot}$ calculations, we also find that fragmentation of the gas occurs, albeit at a much lower level than in the $Z = 10^{-5} Z_{\odot}$ run. The mass functions from these simulations are shown in Figure 4 (middle and right-hand panels), and are again taken when $\sim 19 M_{\odot}$ of gas has been accreted onto the sink particles, the same amount as is accreted by the end of the $Z = 10^{-5} Z_{\odot}$ calculations.

The primordial gas clouds form fewer protostars than the $Z = 10^{-5} Z_{\odot}$ clouds, with the high resolution simulation forming 25 sink particles and the low-resolution simulation forming 22 sink particles. The mass functions are considerably flatter than the present day IMF, in agreement with the suggestion that Population III stars are typically very massive. The fragmentation in the $Z = 10^{-6} Z_{\odot}$ simulation is slightly more efficient than in the primordial case, with 33 objects forming. Again we stress that there is a delay of several local free-fall times between the formation of first and second protostars in these simulations: *without the inclusion of sink particles, we would have missed the formation of the lower mass objects.*

4. CONDITIONS FOR FRAGMENTATION AND CLUSTER FORMATION

We now discuss the physical origin of the fragmentation in the $Z = 10^{-5} Z_{\odot}$ simulation, and investigate the properties of the forming cluster. First, we focus on the distribution of gas in the center of the halo right at the

onset of star formation, i.e. at the time when we identify the first sink particle. Figure 6 shows (a) the distribution of rotational speed L/r relative to the Keplerian velocity $v_{\text{kep}} = (GM/r)^{1/2}$ and (b) the specific angular momentum L in spherical mass shells around the halo center as a function of the enclosed mass. The blue curves denote the $10^{-5} Z_{\odot}$ case, while the red-dashed curves illustrate the behavior of zero metallicity gas, as discussed further below. It is evident that at the time when the first sink particle forms, rotational support plays only a minor role. The rotational velocity of gas in the inner parts of the halo is still sub-Keplerian by a factor of 4 to 5. This will change rapidly in the subsequent evolution as more and more higher angular momentum gas falls to the center. In (c) we plot the enclosed mass and in (d) the spherically averaged density as a function of distance from the center. The density roughly follows a power-law distribution with slope -2 ± 0.1 .

We point out that the properties of the star forming clump in our model are virtually identical to those arising from full cosmological calculations taking into account the combined evolution of baryons and dark matter over time (for comparison, see, e.g. Abel, Bryan, & Norman 2002; Yoshida et al. 2006). If anything, one could argue that the specific angular momentum we consider is somewhat on the low side. We therefore expect that fragmentation will also occur in full cosmological simulations, if these are continued beyond the formation of the very first stellar object (see e.g. Yoshida et al. 2007, for some preliminary evidence of this).

To illustrate how the conditions for cluster formation arise we show in Figure 3 the density distribution perpen-

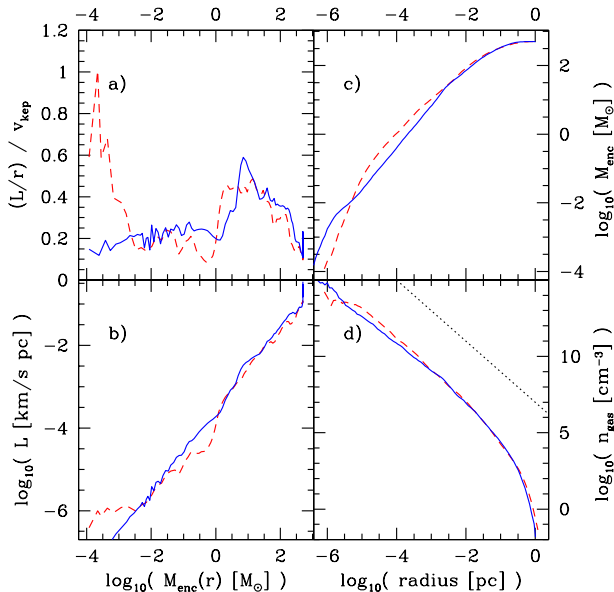


FIG. 6.— (a) Radially-averaged rotational velocity L/r normalized to the Keplerian velocity $v_{\text{kep}} = (GM_{\text{enc}}(r)/r)^{1/2}$ and (b) absolute value of the specific angular momentum L in spherical shells centered on the density peak as function of enclosed mass; (c) $M_{\text{enc}}(r)$ and (d) average local gas density $n_{\text{gas}}(r)$ as function of distance r to the center. Blue (solid line) curves denote gas with $Z = 10^{-5}Z_{\odot}$ and red (dashed line) curves denote gas with $Z = 0$. To guide your eye, a power-law slope of -2 is indicated in (d).

dicular to the rotational axis of the system at different times. In Figure 5, in the top panel, we plot both the mass of gas which resides above a density n as well as the Jeans mass. In the bottom panel, we plot the number of Jeans masses, which is simply the mass at this density (or higher) divided by the corresponding Jean mass.

The fragmentation in the low-metallicity gas (the $Z = 10^{-5}Z_{\odot}$ case) is the result of two key features in its thermal evolution. First, the rise in the EOS curve between densities 10^9cm^{-3} and 10^{11}cm^{-3} causes material to loiter at this point in the gravitational contraction. A similar behavior at densities around $n = 10^3\text{cm}^{-3}$ is discussed by Bromm et al. (2001). The rotationally stabilized disk-like structure, as seen in the plateau at $n \approx 10^{10}\text{cm}^{-3}$ in Figure 3, is able to accumulate a significant amount of mass in this phase and only slowly increases in density. Second, once the density exceeds $n \approx 10^{12}\text{cm}^{-3}$, the sudden drop in the EOS curve lowers the critical mass for gravitational collapse by two orders of magnitude. The Jeans mass in the gas at this stage is only $M_J = 0.01 M_{\odot}$, as visible in the top panel of Figure 5. The disk-like structure suddenly becomes highly unstable against gravitational collapse. We see this when looking at the behavior of the number of Jeans masses N_J above a certain density n in the bottom panel of Figure 5, which shortly after the formation of the first stellar object increases to values as high as $N_J \approx 10^3$. Consequently, the disk fragments vigorously on timescales of several hundred years. A very dense cluster of embedded low-mass protostars builds up, and the protostars grow in mass by accretion from the available gas reservoir. The number

of protostars formed by the end of our simulation (177) is nearly two orders of magnitude larger than the initial number of Jeans masses in the cloud set-up.

Because the evolutionary timescale of the system is extremely short – the free-fall time at a density of $n = 10^{13}\text{cm}^{-3}$ is of the order of 10 years – none of the protostars that have formed by the time that we stop the simulation have yet commenced hydrogen burning, justifying our decision to neglect the effects of protostellar feedback in this study. Heating of the dust due to the significant accretion luminosities of the newly-formed protostars will occur (Krumholz 2006), but is unlikely to be important, as the temperature of the dust at the onset of dust-induced cooling is much higher than in a typical Galactic protostellar core ($T_{\text{dust}} \sim 100\text{K}$ or more, compared to $\sim 10\text{K}$ in the Galactic case). The rapid collapse and fragmentation of the gas also leaves no time for dynamo amplification of magnetic fields (Tan & Blackman 2004), which in any case are expected to be weak and dynamically unimportant in primordial and very low metallicity gas (Widrow 2002).

The cluster forming in our $Z = 10^{-5}Z_{\odot}$ simulation represents a very extreme analogue of the clustered star formation that we know dominates in the present-day Universe (Lada & Lada 2003). A mere 420 years after the formation of the first object, the cluster has formed 177 stars (see Figure 2). These occupy a region of only around 400 AU, or $2 \times 10^{-3}\text{pc}$, in size, roughly a hundredth of the size of the initial cloud. With $\sim 19M_{\odot}$ accreted at this stage, the stellar density is $2.25 \times 10^9 M_{\odot}\text{pc}^{-3}$. This is about five orders of magnitude greater than the stellar density in the Trapezium cluster in Orion (Hillenbrand & Hartmann 1998) and about a thousand times greater than that in the core of 30 Doradus in the Large Magellanic Cloud (Massey & Hunter 1998). This means that dynamical encounters will be extremely important during the formation of the first star cluster. The violent environment causes stars to be thrown out of the denser regions of the cluster, slowing down their accretion. The stellar mass spectrum thus depends on both the details of the initial fragmentation process (e.g. as discussed by Jappsen et al. 2005; Clark & Bonnell 2005) as well as dynamical effects in the growing cluster (Bonnell et al. 2001; Bonnell, Bate & Vine 2004). This is different to present-day star formation, where the situation is less clear-cut and the relative importance of these two processes may vary strongly from region to region (Krumholz, McKee, & Klein 2005; Bonnell & Bate 2006; Bonnell, Larson & Zinnecker 2007).

Dynamical encounters in the extremely dense proto-cluster will also influence the binary fraction of the stars that form. Wide binaries will be rapidly disrupted, and so any binary systems that survive will be tightly-bound close binaries (Kroupa 1998). Recent observations suggest that extremely metal-poor low-mass stars have a higher binary fraction than that found for normal metal-poor stars, and that the period distribution of these binary systems is also skewed towards tight, short-period binaries (Lucatello et al. 2005). Mass transfer from a close binary companion may also be able to explain the extremely high $[C/Fe]$ ratios measured in the most metal-poor stars currently known (Ryan et al. 2005; Komiya et al. 2007). Our results suggest that these stars may originate in conditions similar to those that

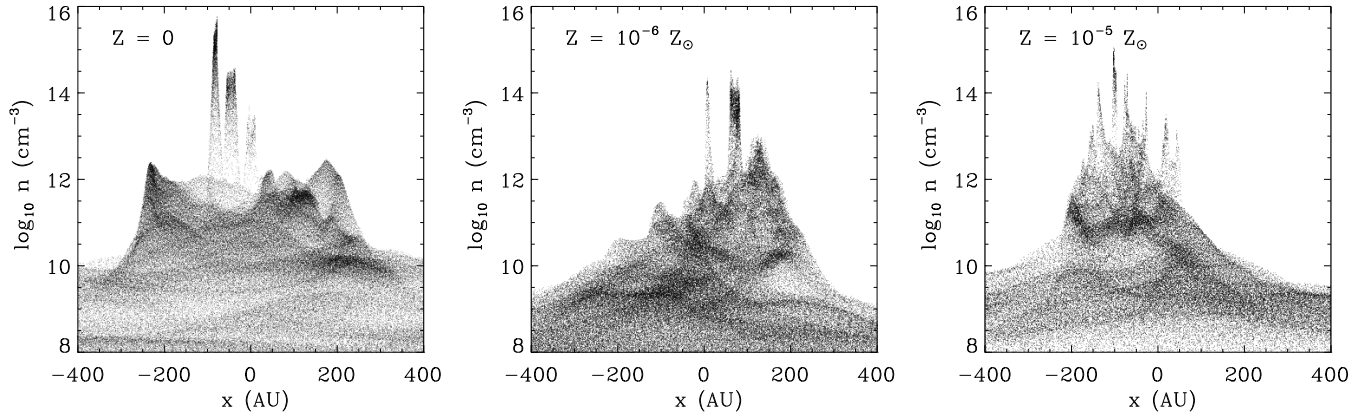


FIG. 7.— Particle densities as a function of position in the low-resolution simulations, for the primordial (left), $Z = 10^{-6} Z_{\odot}$ (middle) and $Z = 10^{-5} Z_{\odot}$ simulations (right). The particles are plotted once the protostars in each simulation have accreted $19 M_{\odot}$ of gas.

we find in our simulations. Further work aimed at improving our understanding of the binary statistics of low-metallicity stars formed by dust-induced fragmentation is clearly required.

As mentioned in Section 3, the primordial and the $Z = 10^{-6} Z_{\odot}$ cases also exhibit some fragmentation. Careful analysis of the Omukai et al. (2005) EOS for zero-metallicity gas shows roughly isothermal behavior in the density range $10^{14} \text{ cm}^{-3} \leq n \leq 10^{16} \text{ cm}^{-3}$, i.e. just before the gas becomes optically thick and begins to heat up adiabatically. Conservation of angular momentum again leads to the build-up of a rotationally supported massive disk-like structure which then fragments into several objects. This is understandable, as isothermal disks are susceptible to gravitational instability (Bodenheimer 1995) once they have accumulated sufficient mass. Further, Goodwin et al. (2004a,b) show how even very low levels of turbulence can induce fragmentation. Since turbulence creates local anisotropies in the angular momentum on all scales, it can always provide some centrifugal support against gravitational collapse. This support can then provide a window in which fragmentation can occur.

In addition to the quasi-isothermal behavior of the gas, both of the $Z \leq 10^{-6} Z_{\odot}$ equations of state from Omukai et al. (2005) also contain a brief phase of cooling during the collapse, which further aids fragmentation. In the primordial case, this occurs very late in the collapse, just above $n = 10^{14} \text{ cm}^{-3}$, and is due to the onset of efficient cooling from H_2 collision-induced emission (Omukai & Nishi 1998; Ripamonti & Abel 2004). In the $Z = 10^{-6} Z_{\odot}$ EOS, the cooling occurs earlier, at around $n = 10^{10} \text{ cm}^{-3}$, and is due to a combination of effects – enhanced H_2 cooling resulting from the rapid increase in the molecular fraction at these densities due to efficient three-body H_2 formation, and rotational and vibrational line cooling from H_2O – that are present in the model of Omukai et al. (2005). One can see the emergence of structure at these densities in the particle plots shown in Figure 7. However, the effect is much less pronounced in the primordial case. Indeed a further low-resolution simulation of the primordial EOS in which this dip was removed yielded almost identical results, forming 17 sink particles

instead of 22, suggesting that the quasi-isothermal nature of the gas is more important than this brief cooling phase.

In comparison to the $Z = 10^{-5} Z_{\odot}$ case, the strength of fragmentation in the $Z \leq 10^{-6} Z_{\odot}$ calculations is weak, and only a few objects form for the combination of total mass ($M = 500 M_{\odot}$), angular momentum ($E_{\text{rot}}/|E_{\text{grav}}| = 0.02$), and level of initial turbulence ($E_{\text{turb}}/|E_{\text{grav}}| = 0.1$) that we adopted in our simulations. Consequently the stars (sink particles) forming in the $Z \leq 10^{-6} Z_{\odot}$ simulations are typically of higher mass than those in the $Z = 10^{-5} Z_{\odot}$ simulations, consistent with the predictions made by Abel, Bryan, & Norman (2002) and Bromm, Coppi, & Larson (2002). Although the recent high-resolution SPH simulation of primordial gas performed by Yoshida *et al.* (2006), which predict a similar EOS to that used in our primordial simulations, find no fragmentation, they do not follow the evolution of the gas beyond the formation of the first collapsing core, since they do not include sink particles in their study, and so they may miss this subsequent phase of fragmentation. However, more recent work Yoshida *et al.* (2007), does show evidence of fragmentation on scales of around 0.1pc.

5. CAVEATS

Although the equations of state taken from Omukai et al. (2005) provide an opportunity for vigorous fragmentation at low metallicities, there are a number of questions which still need to be addressed. One immediate uncertainty is the applicability of the results derived from a 1-zone model to a full three-dimensional collapse calculation, which contains turbulence and thus local anisotropies in velocity and density structure. In particular, the existence of a strict relationship between temperature and density is unlikely, even when the cooling time of the gas is short compared to the dynamical time (Whitehouse & Bate 2006). If the gas were to collapse more slowly than is assumed in the Omukai et al. (2005) calculations, or if the opacity of the gas were to be lower, then less heating would occur prior to the onset of efficient dust cooling.

On the other hand, if the collapse is faster than Omukai et al. (2005) assume or if the gas opacity is greater, then

more heating would occur. Since the amount of heating that occurs during the loitering phase helps to accumulate material at high densities, which then acts as a reservoir for fragmentation, the amount of fragmentation will be sensitive to the thermal evolution of the gas during this phase of the collapse, and is therefore somewhat uncertain. However, we note that unless the temperature dip is eliminated entirely (which seems unlikely), fragmentation will still occur along the lines outlined in this paper. We therefore believe our results to be qualitatively, if not quantitatively, correct.

A related issue is one of dust opacity. In their study, Omukai et al. (2005) use a dust model based on Pollack et al. (1994), which was designed for the study of Galactic dust. However, it is not at all clear that this is the appropriate model to use, given that high-redshift dust is likely to differ significantly from local dust (see e.g. Todini & Ferrara 2001). Schneider et al. (2006) have performed a similar study to that of Omukai et al. (2005), but use a dust model based on the results of Todini & Ferrara (2001) and Schneider, Ferrara, & Salvaterra (2004) in place of the Pollack et al. (1994) dust model. They find that this leads to qualitatively similar behavior to the Omukai et al. (2005) model, but that the onset of effective dust cooling happens at lower metallicity, $Z = 10^{-6} Z_{\odot}$ rather than $Z = 10^{-5} Z_{\odot}$. However, the use of this alternative dust model can also be questioned, since Nozawa et al. (2003) have shown that the composition and properties of the dust produced by population III supernovae are strongly dependent on the (poorly-constrained) degree of mixing assumed to occur in the ejecta, and since the model does not take into account the destruction of grains by thermal sputtering in the reverse shock in the supernova remnant (Bianchi & Schneider 2007), or the growth of grains through accretion or coagulation during the protostellar collapse (see e.g. Flower et al. 2005).

Lastly, the total amount of heating produced by three body H_2 formation is uncertain. This reaction, which takes place primarily at gas number densities between 10^8 and 10^{13} cm^{-3} , is responsible for much of the rise in gas temperature prior to the dust-cooling phase. However, there is a difference of two orders of magnitude between the three-body H_2 formation rate used in the simulations of primordial star-formation performed by Abel et al. (2002) and the most recent theoretical determination by Flower & Harris (2007), with other suggested rates spanning the full range in between. This introduces an additional uncertainty into the thermal evolution of the gas during the high-density loitering phase.

6. CONCLUSIONS

We have performed numerical simulations of star formation in very high density gas (in the range $5 \times 10^5 \leq n \leq 10^{16} \text{ cm}^{-3}$) in the early universe. The aim of the study was to investigate whether the dust-induced fragmentation predicted by Omukai et al. (2005) and Schneider et al. (2002, 2006) does actually occur in realistic sys-

tems, and to begin to constrain the resulting IMF. The major differences of our work from the only previous numerical study of dust-induced fragmentation (Tsuribe & Omukai 2006) are the inclusion of the effects of rotation, which prove to be of vital importance, and the use of sink particles to capture the formation of multiple protostellar objects.

Based on the equations of state reported by Omukai et al. (2005), our results show that fragmentation of protogalactic gas at very high densities above $n_{\text{gas}} = 10^{12} \text{ cm}^{-3}$ is almost unavoidable, as long as the angular momentum is non-negligible. In this case, rotation leads to the build-up of a massive disk-like structure which provides the background for smaller-scale density fluctuations to grow, some of which become gravitationally unstable and collapse to form stars. At metallicities above $Z \sim 10^{-5} Z_{\odot}$ dust cooling becomes effective at densities $n_{\text{gas}} \sim 10^{12} \text{ cm}^{-3}$ and leads to a sudden drop of temperature which in turn induces vigorous fragmentation. A very dense cluster of low-mass protostars builds up, which we refer to as the first stellar cluster. The mass spectrum peaks below $1 M_{\odot}$, which is similar to the value in the solar neighborhood (Kroupa 2002; Chabrier 2003) and is also comparable to the mass of the very low metallicity subgiant stars recently discovered in the halo of our Milky Way (Christlieb et al. 2002; Beers & Christlieb 2005). If the dust induced cooling model proposed by Omukai et al (2005) is accurate, then the high-density, low-metallicity, fragmentation we describe here may be the dominant process which shapes the stellar mass function.

We find that even purely primordial $Z = 0$ gas with sufficient rotation may fragment at densities $10^{14} \text{ cm}^{-3} \leq n \leq 10^{16} \text{ cm}^{-3}$. In this density range, zero metallicity gas is roughly isothermal and the disk-like structure that forms due to angular momentum conservation is marginally unstable. It fragments into several, quite massive objects, thus supporting the hypothesis that metal-free stars should have masses in excess of several tens of M_{\odot} . Similar behavior is found for gas with a metallicity of $Z = 10^{-6} Z_{\odot}$.

The authors would like to thank Kazuyuki Omukai, Tom Abel, Volker Bromm, Robi Banerjee and Mordecai-Mark Mac Low for helpful discussions concerning this topic. In particular, we would also like to thank Naoki Yoshida for many interesting and insightful discussions regarding this paper. All computations described here were performed at the Jülich Multi-processor (JUMP) supercomputer at the John von Neumann Institute for Computing, Research Centre Jülich, Germany. PCC acknowledges support by the Deutsche Forschungsgemeinschaft (DFG) under grant KL 1358/5. SCOG acknowledges travel support from the European Commission FP6 Marie Curie RTN CONSTELLATION (MRTN-CT-2006-035890).

REFERENCES

- Abel, T., Bryan, G. L., & Norman, M. L. 2002, *Science*, 295, 93
 Bate, M. R., Bonnell, I. A., & Price, N. P. 1995, *MNRAS*, 277, 362
 Bate, M. R., & Burkert, A. 1997, *MNRAS*, 288, 1060
 Beers, T. C., & Christlieb, N. 2005, *ARA&A*, 43, 531
 Bianchi, S., & Schneider, R. 2007, *MNRAS*, 378, 973
 Bodenheimer, P. 1995, *ARA&A*, 33, 199
 Bonnell, I. A., Clarke, C. J., Bate, M. R., & Pringle, J. E. 2001, *MNRAS*, 324, 573

- Bonnell, I. A., Vine, S. G., & Bate, M. R. 2004, *MNRAS*, 349, 735
- Bonnell, I. A., & Bate, M. R. 2006, *MNRAS*, 370, 488
- Bonnell, I. A., Larson, R. B., & Zinnecker, H. 2007, *Protostars and Planets V*, B. Reipurth, D. Jewitt, and K. Keil (eds.), University of Arizona Press, Tucson, p.149
- Bromm, V., Ferrara, A., Coppi, P. S., & Larson, R. B. 2001, *MNRAS*, 328, 969
- Bromm, V., Coppi, P. S., & Larson, R. B. 2002, *ApJ*, 564, 23
- Bromm, V. & Loeb, A. 2003, *Nature*, 425, 812
- Bromm, V., & Loeb, A. 2004, *New Astron.*, 9, 353
- Chabrier, G. 2003, *PASP*, 115, 763
- Christlieb, N., Bessell, M. S., Beers, T. C., Gustafsson, B., Korn, A., Barklem, P. S., Karlsson, T., Mizuno-Wiedner, M., & Rossi, S. 2002, *Nature*, 419, 904
- Clark, P. C., & Bonnell, I. A. 2005, *MNRAS*, 361, 2
- Flower, D. R., & Harris, G. J. 2007, *MNRAS*, 377, 705
- Flower, D. R., Pineau des Forêts, G., & Walmsley, C. M. 2005, *A&A*, 436, 933
- Frebel, A., Johnson, J. L., & Bromm, V. 2007, *MNRAS*, 380, L40
- Goodwin, S. P., Whitworth, A. P., Ward-Thompson, D. 2004a, *A&A*, 414, 633
- Goodwin, S. P., Whitworth, A. P., Ward-Thompson, D. 2004b, *A&A*, 423, 169
- Hillenbrand, L. A., & Hartmann, L. W. 1998, *ApJ*, 492, 540
- Jappsen, A.-K., Klessen, R. S., Larson, R. B., Li, Y., & Mac Low, M.-M. 2005, *A&A*, 435, 611
- Lucatello, S., Tsangarides, S., Beers, T. C., Carretta, E., Gratton, R. G., & Ryan, S. G. 2005, *ApJ*, 625, 825
- Komiya, Y., Suda, T., Minaguchi, H., Shigeyama, T., Aoki, W., & Fujimoto, M. Y. 2007, *ApJ*, 658, 367
- Kroupa, P. 1998, *MNRAS*, 298, 231
- Kroupa, P. 2002, *Science*, 295, 82
- Krumholz, M. R., McKee, C. F., & Klein, R. I. 2005, *Nature*, 438, 332
- Krumholz, M. R. 2006, *ApJ*, 641, L45
- Lada, C. J., & Lada, E. A. 2003, *ARA&A*, 41, 57
- Massey, P., & Hunter, D. A. 1998, *ApJ*, 493, 180
- Nozawa, T., Kozasa, T., Umeda, H., Maeda, K., & Nomoto, K. 2003, *ApJ*, 598, 785
- Omukai, K., & Nishi, R. 1998, *ApJ*, 508, 141
- Omukai, K., & Palla, F. 2003, *ApJ*, 589, 677
- Omukai, K., Tsuribe, T., Schneider, R., & Ferrara, A. 2005, *ApJ*, 626, 627
- O'Shea, B. W., & Norman, M. L. 2007, *ApJ*, 654, 66
- Pollack, J. B., Hollenbach, D., Beckwith, S., Simonelli, D. P., Roush, T., & Fong, W. 1994, *ApJ*, 421, 615
- Ripamonti, E., & Abel, T. 2004, *MNRAS*, 348, 1019
- Ryan, S. G., Aoki, W., Norris, J. E., & Beers, T. C. 2005, *ApJ*, 635, 349
- Santoro, F. & Shull, J. M. 2006, *ApJ*, 643, 26
- Schneider, R., Ferrara, A., Natarajan, P. & Omukai, K. 2002, *ApJ*, 571, 30
- Schneider, R., Ferrara, A., & Salvaterra, R. 2004, *MNRAS*, 351, 1379
- Schneider, R., Omukai, K., Inoue, A. K., & Ferrara, A. 2006, *MNRAS*, 369, 1437
- Tan, J. C., & Blackman, E. G. 2004, *ApJ*, 603, 401
- Todini, P., & Ferrara, A. 2001, *MNRAS*, 325, 726
- Tumlinson, J. 2006, *ApJ*, 641, 1
- Tsuribe, T., & Omukai, K. 2006, *ApJ*, 642, L61
- Whitehouse, S. C., & Bate, M. R. 2006, *MNRAS*, 367, 32
- Widrow, L. M. 2002, *Rev. Mod. Phys.*, 74, 775
- Wuchterl, G., & Klessen, R. S. 2001, *ApJ*, 560, L185
- Yoshida, N., Omukai, K., Hernquist, L., & Abel, T. 2006, *ApJ*, 652, 6
- Yoshida, N., Oh, S. P., Kitayama, T., & Hernquist, L. 2007, *ApJ*, 663, 687